

Denoise and Recognition of Friction AE Signal

Deng Aidong and Jiang Zhang
*National Engineering Research Center of Turbo-Generator Vibration,
Southeast University,
China*

1. Introduction

The friction between rotor and stator of a rotating machine is the common fault, as well as a huge problem to be studied and solved. Acoustic emission (AE) technology provides a new solution to friction detection. However, due to that AE signals cause waveform distortion during transmission in complex structure of a rotating machine, and they are interfered by strong noises of operating environment, AE technology is technically challenged in respect of friction detection. It will be an interesting job to discuss new denoise technologies and research steady identification models.

With respect to the problem that friction AE signals generated by rotating machines are easily interfered by strong noises, this Chapter presents a generalized morphological filter (GMF) based on the fundamental morphological transformation and the combination of those transformation of mathematical morphology. GMF adopts gradient method for iterative computation of weight coefficients of generalized morphological open-closing (GMOC) filter and generalized morphological close-opening (GMCO) filter, so as to find out the weight coefficient value to give the best denoise effect. Then the best weight coefficient value will be used for linear combination of generalized morphological filters to achieve the optimal denoise effect.

With respect to identification study, this Chapter presents an AE identification method that combines cepstral coefficient and fractal dimension together as a Gaussian mixture model (GMM) of characteristic parameters. Such identification model will model the probability density functions contained in eigenvectors of different modal waves in friction AE signals, and cluster these eigenvectors. Each clustering will be considered as a multi-dimensional Gaussian distribution function. Take the mean, covariance matrix and probability of each clustering as the training format of every modal wave, and then put the eigenvectors of friction AE signals to be detected into each format during identification. Weigh the likelihood probability of Gaussian model with maximum ratio combination method to obtain a total likelihood probability. Once the value of total likelihood probability is larger than the given threshold, we can be sure that there is friction AE.

The object to be studied in this Chapter is a rotor test bed equipped with friction device, which can simulate different degrees of friction faults. Use broad band AE sensor and high-speed data acquisition card to acquire complete waveforms of friction AE signals, and then superpose noises on friction AE signals acquired for further study.

2. Adaptive generalized morphological filter based on the gradient method (AGMF-G)

Mathematical morphology [1][2][3] applies set theory to image analysis, which processes an image as a whole package of operands without considering the details, or defining each and every image point of such operands. Set theory can provide a relative mathematical system describing image space combination. Therefore, mathematical morphology can be used to analyze geometric characteristics and structure forms of image objects, making it an extremely important tool for image analysis and processing. Currently mathematical morphology has been extensively applied to fields including image processing, pattern identification, computer vision, and among others.

2.1 Fundamental operations of mathematical morphology

Binary image refers to that the grey scale of an image only consists of 0 and 1. Traditional image processing takes 1 as the grey scale of image object, and 0 as the grey scale of background, and notes X as the set composed of those points in image which grey scale is 1. Mathematical morphology image processing mainly analyzes set X . Morphology uses a method of subjective "probe" interacting with objects to analyze X . "Probe" is a set either which is called "structuring element" by morphology and determined by analyst based on analytical purpose. Mathematical morphology has defined two basic transformation types referring to "dilation" and "erosion" respectively.

1. Set A and B as subsets of N -dimensional Euclidean space, and note $A \oplus B$ as A is dilated by B , therefore

$$A \oplus B = \{x \in E^N \mid x = a + b, a \in A, b \in B\} \quad (1)$$

2. Note $A \ominus B$ as A is eroded by B , therefore

$$A \ominus B = \{x \in E^N \mid x - b \in A, a \in A, b \in B\} \quad (2)$$

Based on dilation and erosion these two fundamental operations, we can structure a morphological operation cluster, namely all operations composed of multiple operations and set operations (union set, intersection set, supplementary set, etc.) of these two fundamental operations. Two most important multiple operations are morphological opening operation and morphological closing operation. Generally speaking, dilation and erosion are unrecoverable operations that either erosion first or dilation first is unable to recover the objects, but generate a new morphological transformation.

3. Note $A \circ B$ as opening operation between A and B , therefore

$$A \circ B = (A \ominus B) \oplus B \quad (3)$$

4. Note $A \bullet B$ as closing operation between A and B , therefore

$$A \bullet B = (A \oplus B) \ominus B \quad (4)$$

$A \circ B$ consists of union sets of subsets in A that are congruent to structural element B, or we can say that for each x in $A \circ B$, there is a translational B_y of structural element in A making $x \in B_y$, namely A has a geometric structure no less than B in close proximity to x .

2.2 Grey scale morphology

Grey scale images are the most circumstances in practice. Contrary to binary images, a grey scale image is the one which contains more than two grey scale values of pixels. Normally a real-valued function in consecutive or digital space is used to describe the grey scale images. Serra [3] adopts the concept of function umbra to apply binary morphology to grey scale images, so that a set representation of grey scale images is established.

One-dimensional signals can be represented with a set. One d -dimensional function $f(x)$ can be represented with a $d + 1$ -dimensional set to define its function umbra:

$$U(f) = \{(x, a) : a \leq f(x)\} \tag{5}$$

That is to say, in a d -dimensional space, umbra is the set less than all the points expressed in function $f(x)$. With the concept of function umbra, we may apply binary morphology to grey scale morphology for signal processing. Normally, when $a = -\infty$, function $f(x)$ is able to be restructured by its umbra set, namely:

$$f(x) = \max\{a : (x, a) \in U(f)\}, \quad \forall x \tag{6}$$

Let $f(x)$ as one-dimensional input signal of definition domain $D_f \subseteq E$, and $g(x)$ as structural element of definition domain $D_g \subseteq E$. Dilate or erode the umbra of function $f(x)$ with the umbra of function $g(x)$ to generate the umbra of a new function, which can be directly represented with $U(f \oplus g) = U(f) \oplus U(g)$ and $U(f \ominus g) = U(f) \ominus U(g)$. The formulas for functional operations of dilation and erosion are:

$$(f \oplus g)(x) = \max_y \{f(x - y) + g(y)\} \tag{7}$$

$$(f \ominus g)(x) = \min_y \{f(x + y) - g(y)\} \tag{8}$$

In the formulas above there are $x \in D_f$ and $y \in D_g$. There is a more specific definition of Equations (7) and (8) that set $f(x)$ as a one-dimensional original signal which definition domain is $\{0, 1, \dots, N - 1\}$, set $g(x)$ as a structure element which definition domain is $\{0, 1, \dots, M - 1\}$, and set the origin at 0, so that dilation and erosion can be defined as follows:

$$(f \oplus g)(n) = \max_{\substack{m=0, 1, \dots, M-1 \\ n=0, 1, \dots, N+M-2}} \{f(n - m) + g(m)\} \tag{9}$$

$$(f \ominus g)(n) = \max_{\substack{m=0, 1, \dots, M-1 \\ n=0, 1, \dots, N-M}} \{f(n + m) - g(m)\} \tag{10}$$

Similar to binary morphological transformation, two important morphological operators of grey scale can be obtained through the combination of dilation and erosion of grey scale: opening operation and closing operation, which are defined as follows:

$$(f \circ g)(x) = ((f \ominus g) \oplus g)(x) \quad (11)$$

$$(f \bullet g)(x) = ((f \oplus g) \ominus g)(x) \quad (12)$$

2.3 Morphological filtering

The fundamental concept of morphological filtering is based on the characteristics of geometric structures of signals that it matches or partially amends signals with predefined structural elements to extract signals and suppress noises. Morphological filter is made of fundamental morphological transformation combination.

Opening operation is able to remove isolated structures like titles, burrs and small bridges, as well as suppress peak noises (positive impulse) in signals; while closing operation is able to level up small grooves, holes and small cracks, as well as suppress valley noises (negative impulse) in signals. In order to simultaneously suppress positive and negative impulse noises in signals, we may construct morphological open-closing (OC) filter and morphological close-opening (CO) filter by using structural elements with the same size and through open-closing operation with different order cascades [4][5]. The definitions are as follows:

Set $f(x)$ as input discrete signal and g as structural element, therefore, morphological open-closing filter and morphological close-opening filter shall be defined as follows:

$$Oc(f) = (f \circ g \bullet g)(x) \quad (13)$$

$$Co(f) = (f \bullet g \circ g)(x) \quad (14)$$

Due to anti-expandability of morphological opening and expandability of morphological closing, for a morphological open-closing filter, the opening operation conducted first not only removes positive impulse noises, but also enhances negative impulse noises. If we conduct closing operation with the same structural element, we may not actually remove all negative impulse noises; similarly, a morphological close-opening filter using the same structural element may not actually remove all positive impulse noises. Considering the selection of width of structural element is the major factor to affect denoise, in order to filter impulse interference from data, the width of structural element shall be larger than the width of maximum impulse of data. Therefore, we have to improve these two types of filters that we select structural elements with different sizes based on the definitions of morphological opening operation and morphological closing operation, so that the next structural function will be wider than the previous one. Thus, we may structure generalized morphological open-closing (GMOC) filters and generalized morphological close-opening (GMCO) filters [6] which are defined as follows:

Set $f(x)$ as input discrete signal, g_1 and g_2 as structural elements, and $g_1 \subseteq g_2$, then generalized morphological open-closing filters and generalized morphological close-opening filters shall be defined respectively as follows:

$$GMOC(f) = (f \circ g_1 \bullet g_2)(x) \quad (15)$$

$$GMCO(f) = (f \bullet g_1 \circ g_2)(x) \quad (16)$$

However, due to that generalized morphological filtering method is still composed of opening operation and closing operation, the two types of generalized morphological filters aforesaid still have statistics offset problems causing output amplitude of open-closing filter relatively low, while output amplitude of close-opening filter relatively high. In most circumstances, it's impossible to gain the best filtering effect by using it alone [7]. Considering the amplitude of friction AE signals of rotor varies a lot, and there are multiple noise components in data, we may use a weighted array of these two generalized morphological filters to effectively erase noises. When weight coefficient is 0.5, the weighted array of two filters is:

$$GMF(f) = 0.5 \times GMOC(f) + 0.5 \times GMCO(f) \quad (17)$$

The filter defined by Equation (17) is called generalized morphological filter (GMF).

2.4 Adaptive generalized morphological filter

In a generalized morphological filter, the weight coefficient of both generalized open-closing filter and generalized close-opening filter is 0.5, and such weight coefficient stays the same during filtering process. The fixed weight coefficient makes filtering results hard to adaptively achieve the best. In order to optimize filtering results, we may use gradient method to conduct iterative computation of weight coefficient, so as to obtain the optimal weight coefficient value.

Set input data as $x(n) = s(n) + u(n)$ and $n = 1, 2, \dots, N$. $s(n)$ represents an ideal signal without any noise, while $u(n)$ represents all types of noise interference. The output of generalized open-closing filters and generalized close-opening filters are:

$$y_1(n) = Goc(x(n)) = (x \circ g_1 \bullet g_2)(n) \quad (18)$$

$$y_2(n) = Gco(x(n)) = (x \bullet g_1 \circ g_2)(n) \quad (19)$$

g_1 and g_2 represent structural elements, therefore, filter output is:

$$y(n) = a_1(n)y_1(n) + a_2(n)y_2(n) = \sum_{i=1}^2 a_i(n)y_i(n) \quad (20)$$

Where, $a_i (i = 1, 2)$ represents weight coefficient.

Mean square deviation of output signal is:

$$E[e^2(n)] = E[|s(n) - y(n)|^2] = E\left[\left| s(n) - \sum_{i=1}^2 a_i(n)y_i(n) \right|^2 \right] \quad (21)$$

With gradient method and by gradually amending weight coefficient $a_i (i = 1, 2)$, filter output $y(n)$ can be closest to the ideal signal $s(n)$ with respect to mean square deviation. To simplify the computation, we may replace $E[e^2(n)]$ with the square of a single error sample $e^2(n)$. Then the gradient of $e^2(n)$ to weight coefficient $a_i (i = 1, 2)$ shall be:

$$\nabla e^2(n) = \left[\frac{\partial[e^2(n)]}{\partial a_1(n)} \quad \frac{\partial[e^2(n)]}{\partial a_2(n)} \right]^T = [\text{grad}_1 \quad \text{grad}_2]^T \quad (22)$$

Iterative computation of adaptive generalized morphological filtering based on gradient method is as follows:

Step 1. Conduct generalized open-closing operation and generalized close-opening operation for input signal $x(n)$ to obtain $y_1(n)$ and $y_2(n)$. Therefore, filter output at the k^{th} iteration is

$$y^k(n) = a_1^k(n)y_1(n) + a_2^k(n)y_2(n) = \sum_{i=1}^2 a_i^k(n)y_i(n) \quad (23)$$

Where $a_i^k (i = 1, 2)$ represents weight coefficient at the k^{th} iteration.

Step 2. Single error sample is:

$$[e(n)]^k = y^{k-1}(n) - y^k(n) \quad (24)$$

Replace $s(n)$ with $y^{k-1}(n)$, then the gradient shall be:

$$[\nabla e^2(n)]^k = [\text{grad}_1^k \quad \text{grad}_2^k]^T \quad (25)$$

Step 3. Determine coefficient β_i^k . There are multiple methods to calculate β_i^k , including the famous HS method presented by Hestenes and Steifel [8]:

$$\beta_i^k = \frac{(\Delta \text{grad}_i^{k-1})^T \text{grad}_i^k}{(\Delta \text{grad}_i^{k-1})^T p_i^k} \quad (26)$$

FR method presented by Fletcher and Reeves [9]:

$$\beta_i^k = \frac{(\text{grad}_i^k)^T \text{grad}_i^k}{(\text{grad}_i^{k-1})^T \text{grad}_i^{k-1}} \quad (27)$$

And PRP method presented by Polak, Ribiere and Polyak individually [10][11]:

$$\beta_i^k = \frac{(\Delta \text{grad}_i^{k-1})^T \text{grad}_i^k}{(\text{grad}_i^{k-1})^T \text{grad}_i^{k-1}} \quad (28)$$

Where $\Delta \text{grad}_i^{k-1} = \text{grad}_i^k - \text{grad}_i^{k-1}$. In Equation (26), p_i^k represents the i^{th} component of direction vector at the k^{th} iteration, $i = 1, 2$.

Here we use FR method to calculate coefficient β_i^k .

Step 4. Calculate each component of direction vector $p^k = [p_1^k \quad p_2^k]^T$:

$$p_i^k = -\text{grad}_i^k + \beta_i^k p_i^{k-1} \quad (29)$$

Then weight coefficient shall be:

$$a_i^{k+1} = a_i^k + \mu p_i^k \tag{30}$$

Where μ represents step parameter. The selection of μ will significantly affect filtering results that a relatively big μ will cause convergent oscillation to unstabilize the system, while a relatively small μ will compromise convergent speed of system for weight coefficient can not be effectively adjusted. There is an optimal μ . Fig. 1 shows the schematic diagram of such algorithm.

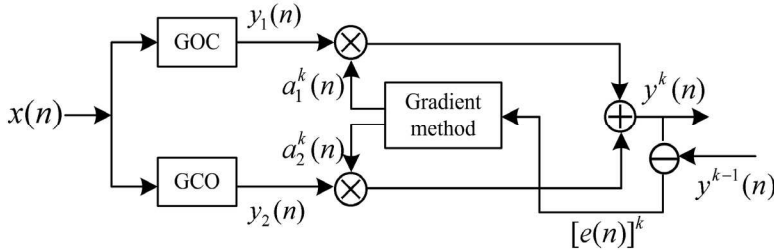


Fig. 1. Schematic Block Diagram of Adaptive Generalized Morphological Filtering Algorithm Based on Gradient Method

In Equations (23) to (30), the superscript k represents the times of iteration. $k = 0, 1, 2, \dots$ and initial weight coefficient is $a_i^0 = 0.5$. Let coefficient $\beta_i^0 = 0$, then $p_i^0 = -grad_i^0$ ($i = 1, 2$). Let $[e(n)]^0 = x(n) - y^0(n)$ for the first iteration. Adaptive amendment of weight coefficient can be achieved through Equations (23) to (30).

2.5 Applications of AGMF-G to denoise of friction AE signals

2.5.1 Experimental conditions

On the rotor friction test bed, the screw on friction support is adjusted to contact the rotor, so as to generate a friction source. We use UT-1000 sensor for the experiment which frequency response ranges from 60kHz to 1000kHz, preamplifier gain is 40dB, and resolution is 18-bit A/D. Rotating speed of rotor on test bed is set at 1500r/min, and sampling frequency is 1MHz. Fig. 2 shows a rotor friction test bed and Fig. 3 shows a friction AE waveform sampled on the rotor test bed.

2.5.2 Selection of structural elements

The results of morphological filtering are greatly related to the structural elements applied. The selection of such structural elements depends on the forms of signals to be processed, which structures shall be as similar to the form characteristics of signals to be analyzed as possible [12]. The selection of structural elements mainly refers to the form, width and height of a structural element. Common structural elements are linear, triangular, circular and polygonal. According to the waveform characteristics of friction AE signals, here we select triangular structural elements to discuss. The width of structural elements g_1 and g_2 in generalized open-closing filter and generalized close-opening filter respectively are 3 and 6.

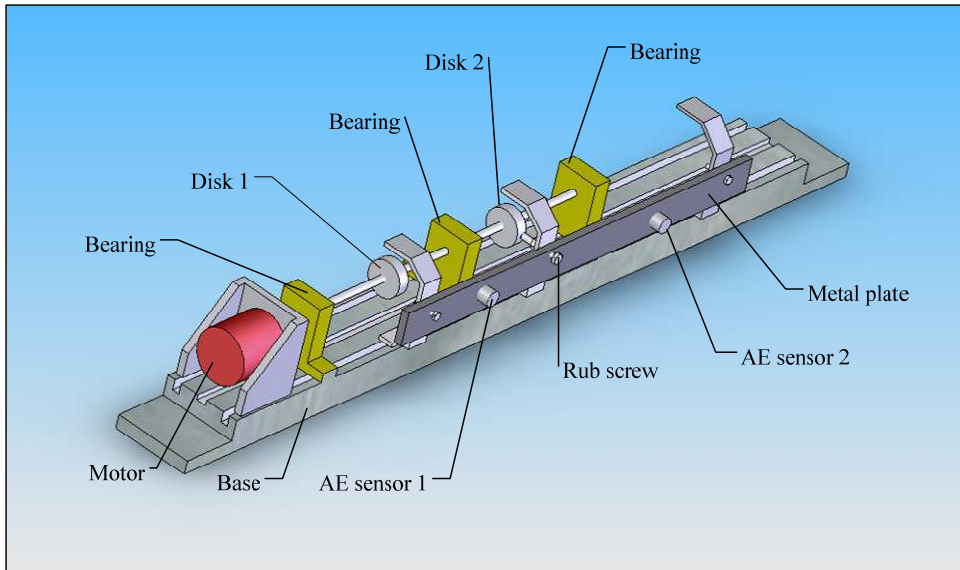


Fig. 2. Rotor Friction Test Bed

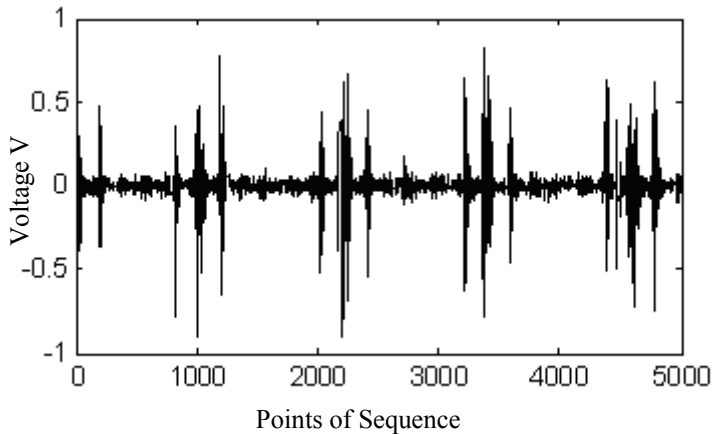


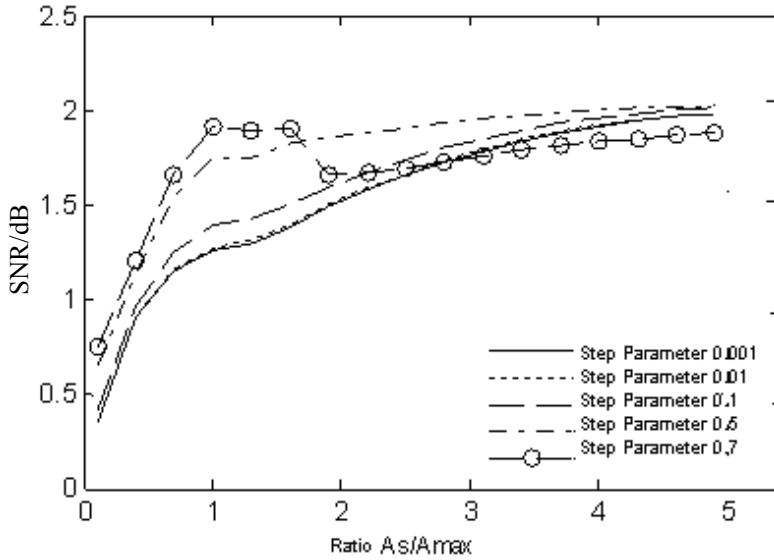
Fig. 3. Friction AE Oscillogram

Experimental simulation indicates that the height A_s of structural element and step parameter μ significantly affect filtering results. The analysis on how height A_s of structural element and step parameter μ affect denoise results is as follows.

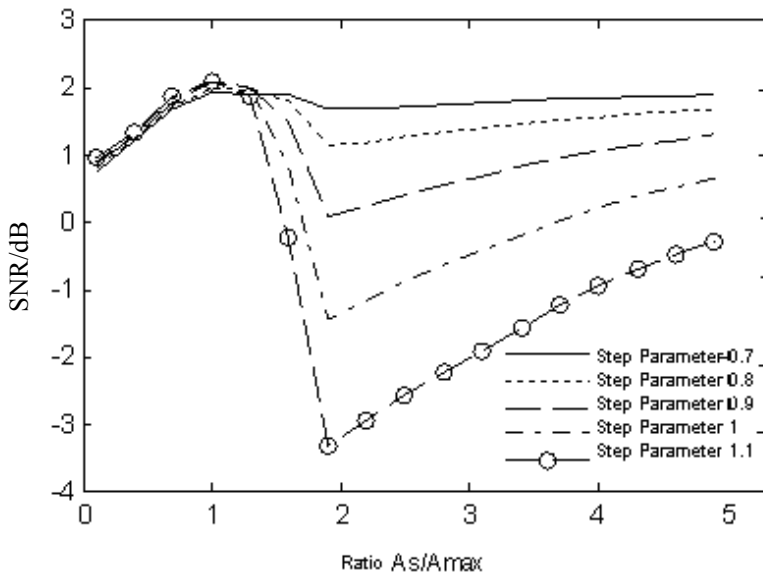
2.5.3 Experimental analysis

The denoise effect of adaptive generalized morphological filter based on gradient method depends on the values of both height A_s of structural element and step parameter μ of a structural element.. Set A_{max} as the amplitude of AE signals. Figs. 4, 5 and 6 show the

relation between ratio A_s / A_{max} and signal-to-noise ratio (SNR) of denoise results when superpose random white noises which SNRs are 0dB, 5dB and 10dB respectively, as well as different step parameters μ .

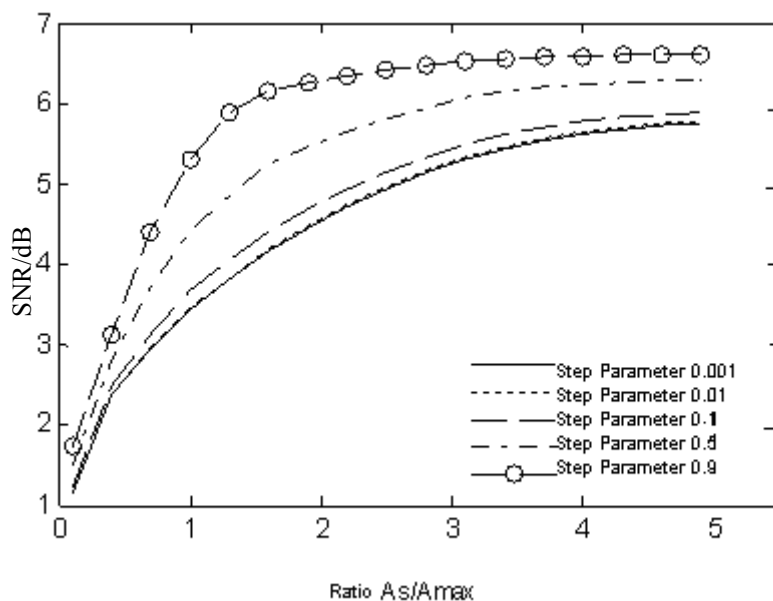


(a) Step Parameter Lower than 0.7

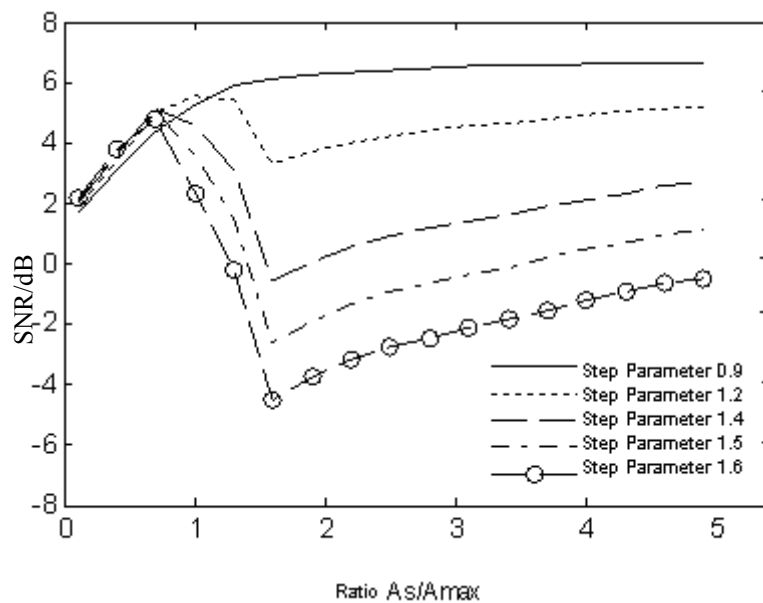


(b) Step Parameter Higher than 0.7

Fig. 4. How Ratio of Step Parameter to A_s / A_{max} Affects Denoise SNR when SNR is 0dB

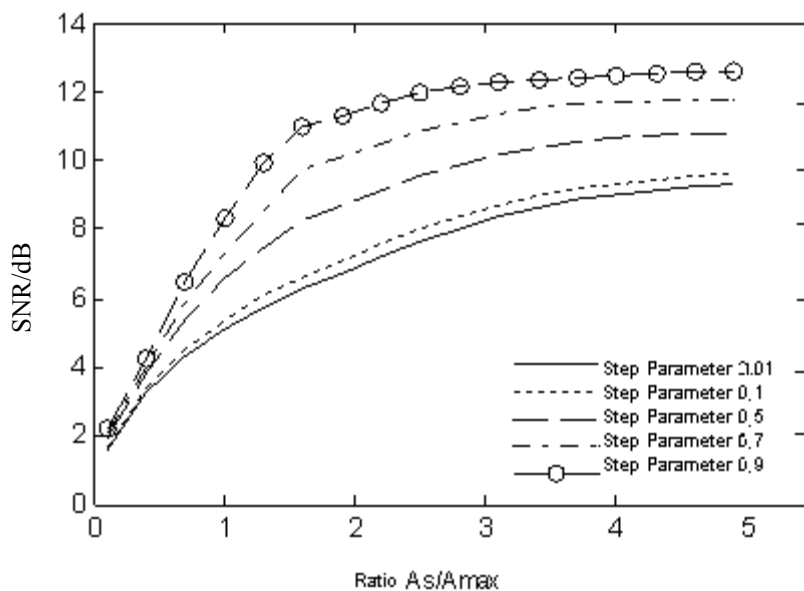


(a) Step Parameter Lower than 0.9

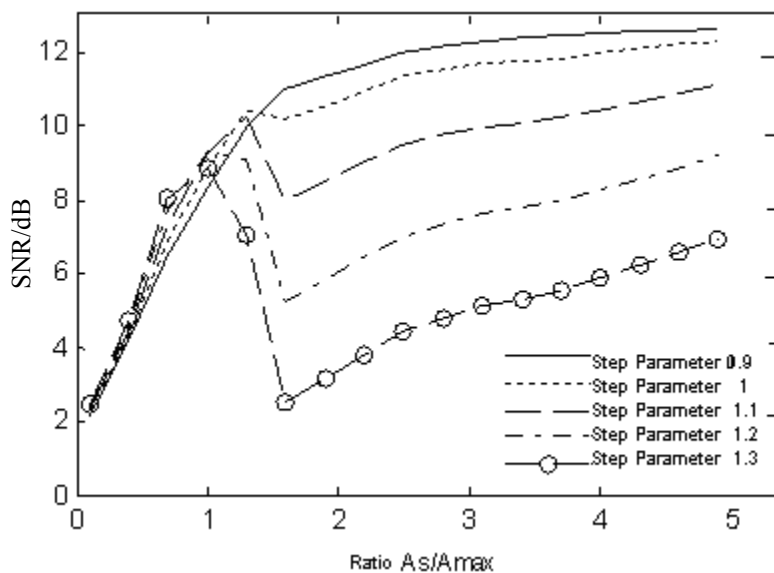


(b) Step Parameter Higher than 0.9

Fig. 5. How Ratio of Step Parameter to A_s/A_{max} Affects Denoise SNR when SNR is 5dB



(a) Step Parameter Lower than 0.9



(b) Step Parameter Higher than 0.9

Fig. 6. How Ratio of Step Parameter to A_s/A_{max} Affects Denoise SNR when SNR is 10dB

Figs. 4-6 indicate that step parameter μ and ratio A_s / A_{max} jointly affect denoise results. There is an optimal step parameter μ that either μ is higher or lower than such optimal value, denoise results are worse than those when μ is at its optimal value. The above figure shows that when SNRs are 0dB, 5dB and 10dB respectively, the optimal values of step parameter μ are 0.7, 0.9 and 0.9 respectively.

The value of ratio A_s / A_{max} also significantly affects denoise results. When step parameter μ is lower than the optimal one, denoise results get better as ratio A_s / A_{max} increases, see Figs. 4(a), 5(a) and 6(a). However, no matter which value of ratio A_s / A_{max} is, denoise results are the best when μ is at its optimal value. When step parameter μ is higher than the optimal one, denoise SNR drops first and then increases as ratio A_s / A_{max} increases, meaning that denoise results vary, see Figs. 4(b), 5(b) and 6(b). However, no matter which value of ratio A_s / A_{max} is, denoise results are inevitably worse than those when μ is at its optimal value.

Therefore, denoise results are ultimately determined by whether step parameter μ is at its optimal value. When step parameter μ is at its optimal value, denoise results get better as ratio A_s / A_{max} increases, see the curves when step parameters μ are 0.7, 0.9 and 0.9 respectively in Figs. 4, 5 and 6. As ratio A_s / A_{max} keeps increasing, the amplitude of denoise SNR tends to 0, which makes few denoise differences. If step parameter μ is at its optimal value, the minimum ratio A_s / A_{max} that makes the amplitude of denoise SNR tends to 0 is the optimal A_s / A_{max} . Figs. 4-6 show that when noise SNRs are 0dB, 5dB and 10dB, optimal ratios A_s / A_{max} are 1, 3 and 4 respectively.

Table 1 indicates the comparison of performances among four denoise algorithms including GMOC, GMCO, GMF and AGMF-G, from which we find that denoise results obtained with AGMF-G is better than those with other three denoise algorithms.

Input Noise/dB	SNR/dB			
	GMOC	GMCO	GMF	AGMF-G
0	0.5002	0.2943	1.2596	1.9201
5	3.3396	2.7512	5.2581	6.5238
10	7.3927	5.9341	9.4739	12.4047

Table 1. Performance Comparison of Friction AE Signal Denoise Algorithms of Morphological Filtering at Different SNRs

3. Identification of friction AE based on GMM

3.1 Modal Acoustic Emission (MAE) and Extraction of Characteristic Parameters

MAE is a type of AE signal processing technology based on guided wave theory [13][14]. MAE thinks that the elastic waves generated by AE sources in materials being detected under loading effect are guided wave signals with diversified frequencies and modes, waves with different modes have different transmission speed and frequencies in transmission media, and some modal waves have frequency dispersion effect [15]. By acquiring AE signals with high-resolution broad band sensor, we may find out the composition mode in AE wave, so that we can connect these modal waves with AE source

mechanism to provide prior knowledge for AE signals judging fault-source mechanism (namely fault type identification). Because different modal waves have different transmission speeds, positioning accuracy will be significantly improved if we use the same modal wave as basis during positioning process. Besides, a large number of non-AE sources or noises do not contain the characteristics of modal waves in AE signals, therefore, it'll be easy to distinguish AE signals from noises.

In this section, we analyze modal characteristics of AE waves during collision and friction excitation, as well as transmission characteristics of AE waves in two different routes of rotor bed. We propose use a mixed parameter composed of logarithmic cepstral parameter and fractal dimension as characteristic parameters of AE signal identification, so as to establish an AE signal identification system of GMM.

According to MAE theory, AE signal $\xi(t)$ received by the sensor can be

$$\xi(t) = \sum_{i=0}^{N-1} \alpha_i \xi_i(t - \tau_i) \quad (31)$$

In the above equation, AE signal $\xi(t)$ is superposed by N modal waves $\xi_0(t - \tau_0), \xi_1(t - \tau_1), \dots, \xi_{N-1}(t - \tau_{N-1})$, and τ represents the time delay from modal wave ξ_i to sensor. Set a_i as 0 or 1. If it is 0, then it means that the sensor doesn't receive such modal wave. $\xi_i(t)$ represents a narrow band random process, namely

$$\xi_i(t) = \xi_{ci}(t) \cos \omega_i t - \xi_{si}(t) \sin \omega_i t \quad (32)$$

$\xi_{ci}(t)$ and $\xi_{si}(t)$ represent in-phase component of quadrature component of narrow band random process $\xi_i(t)$, and ω_i represents its central angle frequency. Equations (31) and (32) show that in a frequency domain, an AE source signal can be considered as the sum of multiple separable narrow band random processes. All modal waves have different speeds during transmission process. Due to frequency dispersion and attenuation, as well as these modal waves start to separate as transmission distance increases, some modal waves will disappear. Thus, we may construct a group of filters with central frequency of modal wave as the center, and band width no more than that of a narrow band random process. For modal waves vary slowly in a frequency domain, energy output of filters also vary slowly. While noises and interference vary randomly, we may distinguish AE signals from noises with the energy output by signals coming through this group of filters.

When a friction fault occurs in rotor system, AE waveforms only show burst characteristics for simple-point friction, while common AE waveforms generated by partial friction show continuous characteristics. Due to waveform distortion and attenuation during transmission, it's impossible for time domain parameter to effectively describe signals, so that intrinsic characteristics of signals can only be identified through time-frequency conversion.

3.1.1 Extraction of cepstral coefficient

AE source signals reach the sensor through transmission in material media, signals received by the sensor are not only affected by media channels, but also present multi-path effects. Therefore, AE signals received by the sensor are affected by multiplicative interference of the channel that characteristics of AE signals and multiplicative interference must be separated

with signal processing. Traditional denoise methods can only process additive interference, while homomorphic filtering especially cepstral technology can obtain excellent results.

Cepstrum is able to interpret relevant characteristics and compensate the distortion of convolutional channels, and it's also able to separate and extract original signals as well as transmit system characteristics, which shows an outstanding robustness in a noise environment. Besides, based on first-order statistical quantity, cepstrum is able to suppress noises [16]. Here we use cepstral coefficient as characteristic quantity of identification model.

The process of extracting cepstral coefficient is shown in Fig. 7.

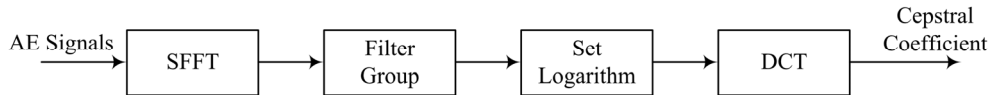


Fig. 7. Extraction of Cepstral Coefficient

Step 1. Conduct short-time Fourier transform (STFT) to AE source signal $\xi(t)$ to obtain its frequency spectrum.

$$X(k, \omega_k) = \sum_{m=-\infty}^{+\infty} \xi[m]w[k-m]\exp(-j\omega_k m) \quad (33)$$

Step 2. Conduct bandpass filtering to energy spectrum in frequency domain with a group of triangular filters. This can be considered as weighing amplitude spectrum with frequency responses of a group of filters. Weighted energy spectrum $E_{\text{mel}}(k)$ refers to Equation (34). Central frequencies of this group of bandpass filters are in a logarithmic scale order, and two bottom point frequencies of filter triangles are equal to the central frequencies of two adjacent filters. Generally, set the number of filters N as 24.

$$E_{\text{mel}}(k) = \frac{1}{A_l} \sum_{k=L_l}^{U_l} |V_l(\omega_k)X(k, \omega_k)|^2 \quad (34)$$

$$k = 1, 2, \dots, N$$

$$A_l = \sum_{k=L_l}^{U_l} |V_l(\omega_k)|^2 \quad (35)$$

In Equation (35), $V_l(\omega)$ represents the frequency response of the l^{th} logarithmic scale filter, and L_l and U_l represent the minimum frequency and the maximum frequency of each filter in a non-zero value-taking interval. A_l is introduced mainly for normalized processing of filters based on band width.

The test shows that the main frequency of rotor friction AE signals ranges from 5kHz to 500kHz. Frequency points contribute differently to AE judgment. HF signals have bigger attenuation during transmission, so the proportion of HF components shall be reduced. Introduce a logarithmic function so that the central frequency of a filter can be:

$$\frac{\ln[1 + a(f_i - f_{\min}) / (f_{\max} - f_{\min})]}{\ln(1 + a)} = \frac{i}{24}, \quad i = 1, 2, \dots, N \quad (36)$$

In Equation (36), a represents coefficient ($a > 0$), f_i ($i = 1, 2, \dots, N$) represents central frequencies of N filters, and f_{\min} represents lower frequency limit. Due to that low frequency range (below 100kHz) is interfered by other industrial noises, therefore, here we take 100kHz. f_{\max} represents upper frequency limit which is 300kHz here.

With Equation (36), we can obtain

$$f_i = \left\{ \frac{\left[\exp\left(\frac{i}{24} \ln(1 + a)\right) - 1 \right] \times 200}{a} + 100 \right\} \text{kHz} \quad (37)$$

Set $N=24$ in practical. The bigger a is, the lower LF filter band width is, and the higher HF filter band width is. Set $a=10$ for identification system analysis later on.

Step 3. Set a logarithm for the output of filter group, and then conduct discrete cosine transform (DCT) of $2N$ points to obtain an modificatory cepstral parameter.

$$C_n = \sum_{k=1}^N \log E_{\text{mel}}(k) \cos[\pi(k - 0.5)n / N], \quad n = 1, 2, \dots, L \quad (38)$$

In Equation (38), L represents the number of cepstral coefficients, which normally is set to be 12-16, and here we take $L=12$. For 0-order cepstral coefficient represents frequency spectrum energy, we don't use 0-order cepstral coefficient for measurement and definition of spectral distortion.

3.1.2 Fractal dimension extraction of AE waveforms

Friction AE signals of rotor system possess fractal characteristics. Fractal dimension not only can be considered as a characteristic parameter of friction AE signal identification, but also can be considered as an index to determine the intensity of friction. DENG Aidong [17] presented a fractal dimension algorithm based on wave length. He used a box which dimension was δ to cover the whole AE wave curve. Set $N_\delta(F)$ as the smallest number of curves covered by the box which side length is δ , and set $l_i(\delta)$ as the curve length in the i th box, so that AE wave length can be

$$L(\delta) = \sum_{i=1}^{N_\delta(F)} l_i(\delta) \quad (39)$$

The curve length $l_i(\delta)$ inside each box is equivalent to: $l_i(\delta) = k_1 \delta$ where k_1 represents coefficient that can be set between 1 and 1.5 in practical. Set δ_0 as k times of the minimum sampling interval (namely the box which dimension is δ): $\delta_0 = k \delta$ where k is an integer. The algorithm is as follows

$$D = A - \frac{\ln L(\delta)}{\ln \delta_0} - \frac{B\delta_0}{L(\delta)\ln L(\delta)} \quad (40)$$

In Equation (40), D is called the wave length fractal dimension (WLFD), where $A = 1 + \ln k_1 / \ln \delta_0$, $B = r(\delta / \delta_0 - 1)$, and parameters A, B, k are determined with fractal Brownian curve.

In practical, we may conduct framing processing to noise-bearing friction AE signals that have been sampled and quantified. Because the number of sample points in each frame is relatively low, it causes fractal dimension of frame varying greatly and high variance. In order to improve the accuracy of fractal dimension, we may conduct medium filtering to fractal dimension of frame first to filter HF components, so that the variance of fractal dimension can be reduced. For noise-bearing data in each frame, we may equally divide them into m (m is an odd number) data segments which will be in $D_{i-v}, \dots, D_{i-1}, D_i, D_{i+1}, \dots, D_{i+v}$ order. Set the data which serial number is in the middle as output of medium filtering

$$Y_i = \text{Med}\{D_{i-v}, \dots, D_{i-1}, D_i, D_{i+1}, \dots, D_{i+v}\}, \quad v = \frac{m-1}{2} \quad (41)$$

3.2 GMM-based identification system

GMM approaches any distribution through linear combination of several Gaussian probability density functions that it can well describe the spatial distribution and its characteristics of training data in parameter space. In a friction AE identification system, GMM models probability density functions contained in eigenvector of different modal waves, and clusters through these eigenvector. Each clustering can be considered as a multi-dimensional Gaussian distribution function. Calculate the mean, covariance matrix and probability of each clustering and set as the training format of each modal wave, and then put the characteristic sequences of AE signals to be detected into the format of each modal wave to obtain the maximum posterior probability, namely the modal wave identified by correspondence. Here we only have to know if AE signals exist rather than understand the details of modal waves at receiving end. Therefore, combine the output likelihood ratios of all modal wave models to obtain a total likelihood ration, and then judge based on such total likelihood ratio. See Fig. 8 for identification system model.

A model is composed of training stage and identification stage. Although AE signals are non-stationary, they can be considered stationary in a short time window that can be analyzed with stationary process. Therefore, we may divide AE signals into several frames with short time intervals, and then we use overlapping segmentation method to achieve smooth transition between frames. Here we divide the whole AE signal sequence to be trained or identified into several short time intervals that each with 512 points and 50% overlapping.

Based short time intervals, we extract a 12-dimensional logarithmic cepstral parameter (remove No. 0-dimensional cepstral parameter) and fractal dimension of wave length according to Equations (38) and (41) to form a 13-dimensional AE signal characteristic parameter.

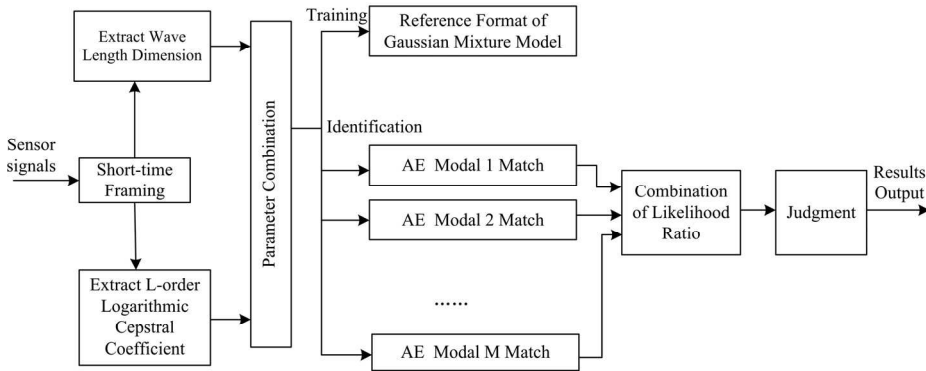


Fig. 8. GMM-based AE Identification Model

In a rotor system, AE waves may show up in multiple patterns during transmission including flexural waves, spreading waves and torsional waves, so that each type of wave in the model can be trained and identified with a corresponding Gaussian model.

GMM is the weighted sum of M modal densities. The likelihood ratio corresponding to vector \bar{x} extracted from AE signals can be expressed as M Gaussian components

$$p(\bar{x} | \lambda) = \sum_{i=1}^M a_i b_i(\bar{x}) \tag{42}$$

Here \bar{x} represents a D -dimensional random vector; $b_i(\bar{x})$ ($i=1, \dots, M$) represents density function of each modal; and a_i ($i=1, \dots, M$) represents the weight of i^{th} Gaussian component. Each modal density represents a Gaussian function of D -dimensional variable with respect to mean vector $\bar{\mu}_i$ and covariance matrix Σ_i

$$b_i(\bar{x}) = \frac{1}{(2\pi)^{D/2} |\Sigma_i|^{1/2}} \exp\left\{-\frac{1}{2}(\bar{x} - \bar{\mu}_i)' \Sigma_i^{-1} (\bar{x} - \bar{\mu}_i)\right\} \tag{43}$$

Where mixture weight meets the following condition

$$\sum_{i=1}^M a_i = 1$$

Complete parameters of AE identification model of Gaussian mixture density are obtained through mean vectors, covariance matrixes and parameterized mixture weights of all modal densities. Together, these parameters can be expressed as

$$\lambda_i = \{a_i, \bar{\mu}_i, \Sigma_i\}, \quad i = 1, \dots, M \tag{44}$$

Each modal wave can be expressed as one GMM and its model parameter λ_i . For the sequence of T test vectors $\mathbf{X} = (\bar{x}_1, \bar{x}_2, \dots, \bar{x}_T)$, its GMM probability is

$$P(\mathbf{X} | \lambda) = \prod_{i=1}^T p(\bar{x}_i | \lambda) \tag{45}$$

AE signals may go through modal transform and multi-modal coexistence during a certain period of time. The optimization can not be achieved with Equation (45). Therefore, the following shall be conducted

$$p(\bar{\mathbf{x}}_t, \lambda) = \sum_{i=1}^M a_i p(\bar{\mathbf{x}}_t | \lambda_i) \quad (46)$$

Equation (46) adopts the combination of maximum ratios. a_i represents the weight of branch channel, related to the probability $p(\bar{\mathbf{x}}_t | \lambda_i)$ of branch channel. Branch channel with bigger probability has larger weight coefficient, vice versa. To simplify the analysis, we may set $a_i = p(\bar{\mathbf{x}}_t | \lambda_i)$, thus Equation (46) may be

$$p(\bar{\mathbf{x}}_t, \lambda) = \sum_{i=1}^M p(\bar{\mathbf{x}}_t | \lambda_i)^2 \quad (47)$$

Put likelihood probability $p(\bar{\mathbf{x}}_t | \lambda)$ of each frame obtained with Equation (46) into Equation (45), we may get a total likelihood probability $P(\mathbf{X} | \lambda)$. It can be considered that AE signals exist if $P(\mathbf{X} | \lambda)$ is larger than the threshold.

3.3 Test analysis

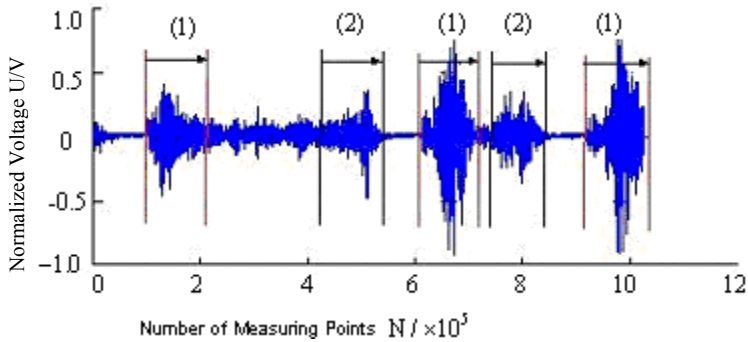
3.3.1 Test analysis on GMM input

See Fig. 2 for test device. Set sampling set as 2MHz, and set the number of sampling data points of single trigger as 32768.

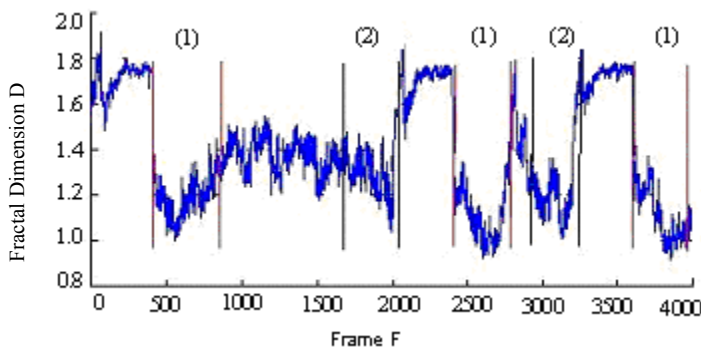
When friction occurs in the rotor, such friction actually contains tangential friction and normal collision force. AE signals we observe are waveforms stimulated by the combination of collision and friction between rotor and stator. Experimental research shows that AE modal waves stimulated by collision and friction respectively are different that collision mainly stimulates flexural waves while friction mainly stimulates spreading waves[18]. And it's hard to distinguish these two types of waves in friction AE signals acquired in practice. For the sake of simplification, we may generally classify friction AE signals based on their waveforms during transmission and their fractal dimension curves in certain structures and distances, so as to determine GMM model input type.

Fig. 9 and Fig. 10 indicate friction AE waveforms and fractal dimension curves of waveforms at distance end and near end respectively, from which we find that fractal dimension can effectively distinguish AE signals and noises. When AE signals are transmitted far enough, some frequency components are separated, which means that although there are waveform peaks, waveforms stretch a lot and are relatively flat. With fractal curves, we may divide them into two modal types as source input of identification model, see Fig. 9.

If friction AE source is at the near end of sensor, the in respect of waveforms, we find that almost all modal components gather together, and the sharp composite wave formed contains plenty of frequency components, see Fig. 10. Therefore, the whole wave packet shall be input as a model source of GMM.



(a) AE Signal Waveform at Distance End and Division of Two Modals



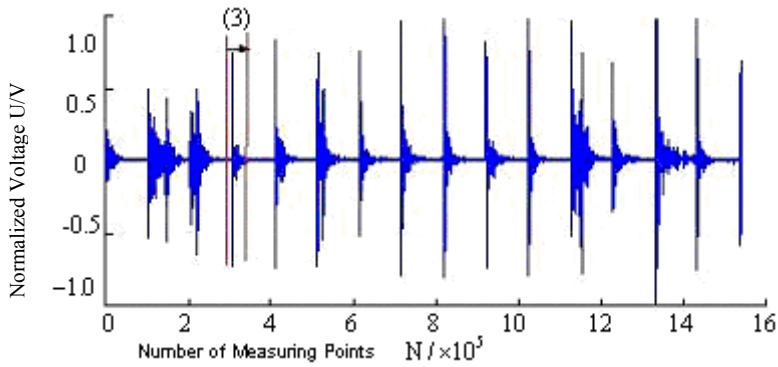
(b) Logarithmic Wave Length Dimension Curve of AE Signal Waveform at Distance End and Division of Two Modals

Fig. 9. Modal Characteristics of AE Waveforms at Distance End

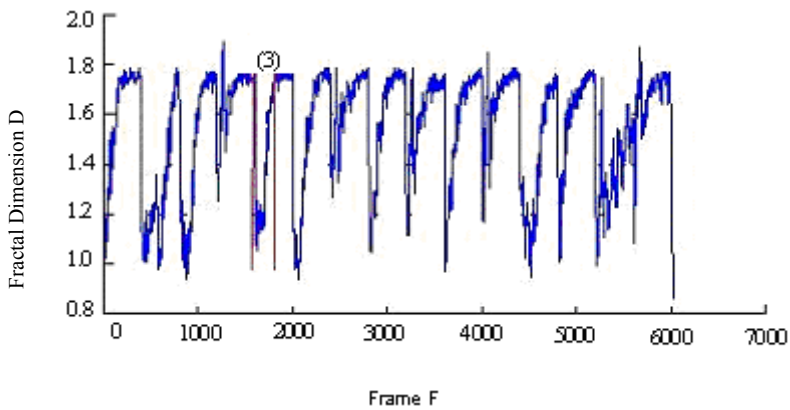
Based on the analysis above, friction AE waveforms can be classified into three models. Take the situation of no AE into consideration, we may set the number of models as $M = 4$.

3.3.2 Performance analysis on AE identification model under noise environment

Acquire near end AE data 3cm away from friction source and distance end AE data 40cm away from friction source for 10 seconds on rotor friction test bed for training (rotating speed = 1450r/min). Then acquire AE test data for 10 seconds when rotating speeds are 500r/min and 1800r/min respectively. Superpose Gaussian white noises and workshop noises with different SNRs on all test data, and then identify them with the above mentioned model. For results, see Fig. 11. It shows that identification rate at near end is higher than that at distance end, identification performance under Gaussian white noise environment is better than that under workshop noise environment, and identification rates at different rotating speeds are almost the same.



(a) AE Signal Waveform at Near End



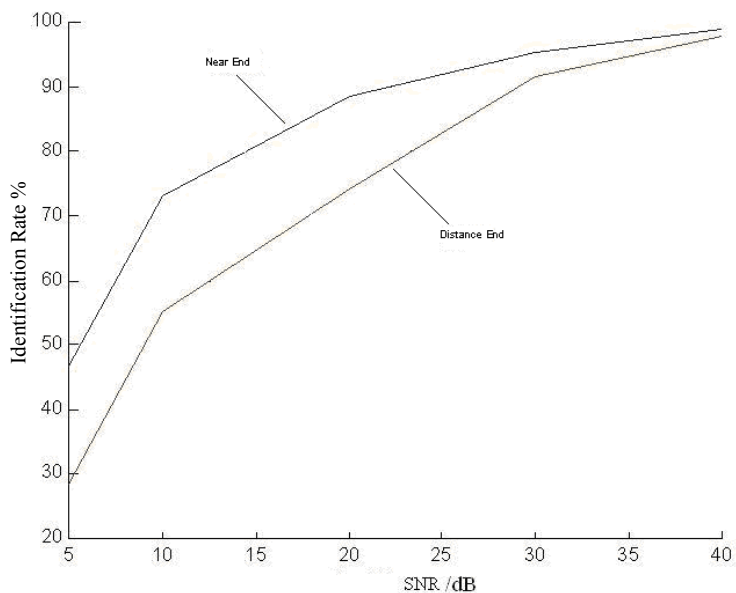
(b) Wave Length Fractal Dimension Curve of AE Signal at Near End

Fig. 10. Modal Characteristics of AE Waveforms at Near End

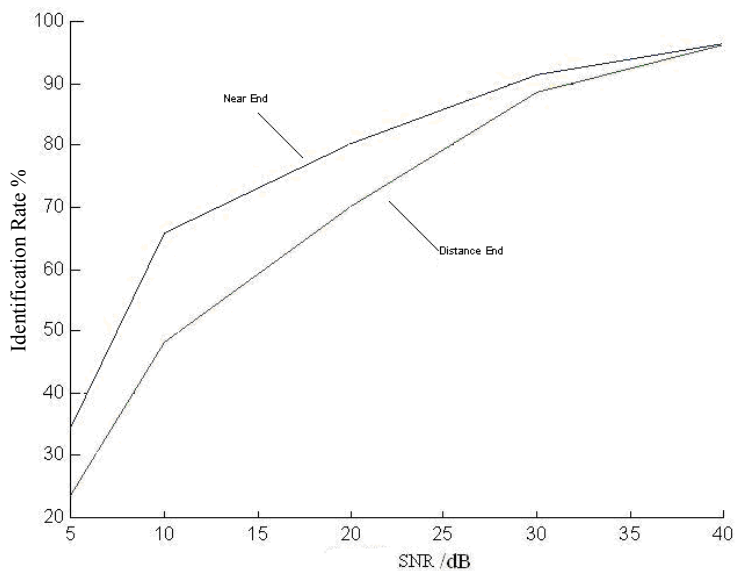
Compare the identification system of mixed characteristic parameters combining 12-order and fractal dimension to the identification system of mixed characteristic parameters only using 12-order cepstral coefficients. Table 2 shows that the identification performance of former one is improved at different SNRs, especially at a low SNR it's improved significantly. This means that mixed characteristic parameters not only effectively improves identification performance, but also are able to suppress Gaussian white noises to a certain degree.

Characteristic Parameters	Identification Rate r/(%)				
	5dB	10dB	20dB	30dB	∞
Cepstral Coefficient	36.7	62.9	81.1	86.2	96.8
Cepstral Coefficient + Fractal Dimension	46.2	74.3	86.9	95.4	98.1

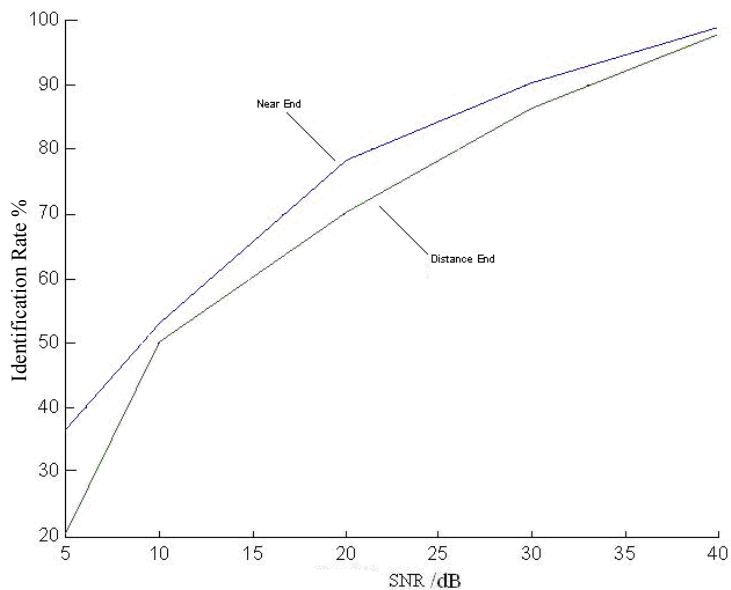
Table 2. Comparison of Identification Rates under Gaussian White Noise Environment Based on Different Characteristic Parameters and at Different SNRs



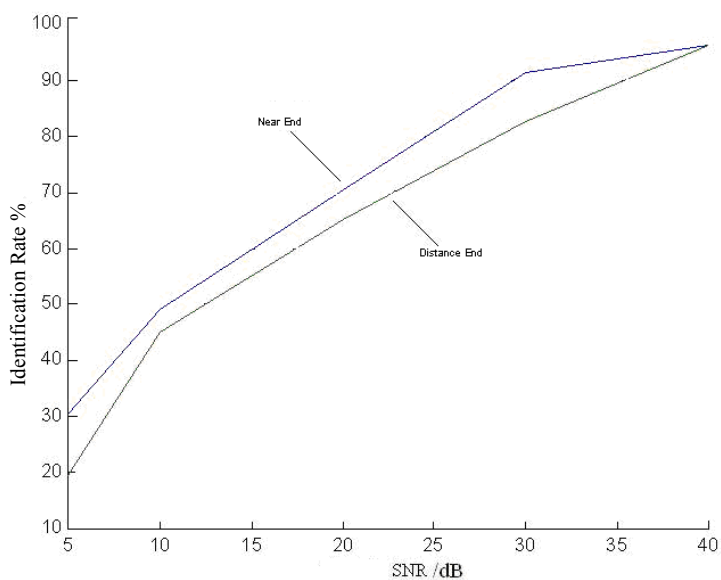
(a) Friction Identification Rate at Different SNRs and Under Gaussian White Noise Environment (500r/min)



(b) Friction Identification Rate at Different SNRs and Under Gaussian White Noise Environment (1800r/min)



(c) Friction Identification Rate at Different SNRs and Under Workshop Noise Environment (500r/min)



(d) Friction Identification Rate at Different SNRs and Under Workshop Noise Environment (1800r/min)

Fig. 11. AE Identification Rates under Different Noise Environments

4. Conclusion

This Chapter presents an adaptive generalized morphological filtering denoise algorithm based on gradient method, and has applied it to denoise of friction AE signals. Through experimental analysis, we may select appropriate step parameter μ and ratio A_s / A_{max} . Denoise effects generated by adaptive generalized morphological filtering algorithm based on gradient method are better than those generated by other traditional morphological filtering algorithms, which is a new solution to denoise of AE signals. In addition, the selection of optimal step parameter μ still has normal statistics characteristics that it needs to be determined through multiple computations and experiments. Therefore, this filtering algorithm still can be improved.

We have classified the modals of AE waveforms based on how friction AE signals transmit in a rotor system structure. Then we combine cepstral coefficient and fractal dimension of each modal wave as mixed characteristic parameters to represent friction AE signals, and then construct a friction AE identification system of GMM. Test results show that this model is able to obtain a relatively high identification rate under noise environment, and is able to suppress Gaussian white noises to a certain degree, which can be used as an approach to identify friction.

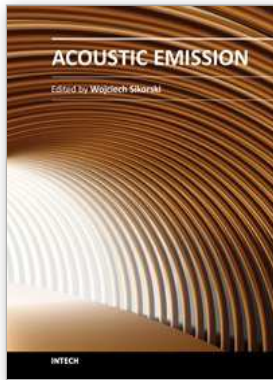
5. Acknowledgement

This work was supported by the National Natural Science Foundation of China (51075068).

6. References

- [1] J. Serra, L. Vincent. An Overview of Morphological Filtering. *Circuits, Systems, Signal Process.* 1992, 11(1): 47-108.
- [2] G. Matheron. *Random Sets and Integral Geometry*. New York: Wiley, 1975.
- [3] J. Serra. *Image Analysis and Mathematical Morphology*. New York: Academic, 1982.
- [4] Maragos P, Schafer R W. Morphological Filters-Part I: Their Set Theoretic Analysis and Relations to Linear Shift Invariant Filters. *IEEE Trans. on Acoustics, Speech and Signal Processing*, 1987, 35(8), 1153~1169.
- [5] Maragos P, Schafer R W. Morphological Filters-Part II: Their Relations to Median, Order-Statistics, and Stack Filters, *IEEE Trans. on Acoustics, Speech and Signal Processing*, 1987, 35(8), 1170~1184.
- [6] Zhao Chunhul, Sun Shenghe. An Adaptive Weighted Combination Filter Based on Morphological Opening and Closing Operators. *Acta Electronica Sinica*, 1997, 25(6): 107-111.
- [7] Hu Aijun, Tang Guiji, An Liansuo. De-noising Technique for Vibration Signals of Rotating Machinery Based on Mathematical Morphology Filter. *Chinese Journal of Mechanical Engineering*, 2006, 42(4): 127-130.
- [8] Hestenes M R, Stiefel E L. Methods of Conjugate Gradients for Solving Linear Systems. *Journal of Research of the National Bureau of Standards*, 1952, 5(2):409-432.
- [9] Fletcher R, Reeves C. Function Minimization by Conjugate Gradients. *Computer Journal*, 1964, 7(1): 149-154.

- [10] Polak B, Ribiere G. Note Surla Convergence des Methodes de Directions Conjuguees. *Rev Francaise Imofrmmat Recherche Opertionelle*, 1969, 16(1): 35-43.
- [11] Polyak B T. The Conjugate Gradient Method in Extreme Problems. *USSR Computational Mathematics and Mathematical Physics*, 1969, 9(1): 94-112.
- [12] Zhao Wenbin, Zhou Xiaojun, Lin Yong. Application Research of Generalized Morphological Filter in Vibration Signal Processing. *Transactions of the CSAE*, 2008, 24(6):203-205.
- [13] Gorman M R. Plate Wave Acoustic Emission. *Journal of Acoustic Society of America (JASA)*, 1991, 90(1): 358-364.
- [14] Prosser W H, Gorman M R. Extensional and Flexural Waves in a Thin-Walled Graphite/Epoxy Tube. *Journal of Compos Mater* 1992, 26(20): 2016-2027.
- [15] Dunegan H L. Modal Analysis of Acoustic Emission Signals. *Journal of Acoustic Emission*. 1998, 15(1): 1-4.
- [16] Kotnik B, Vlaj D, Kacic Z. Robust MFCC Feature Extraction Algorithm Using Efficient Additive and Convolutional Denoise Procedures//*ICSLP'02 Proceedings*, Denver, USA, 2002: 455-448.
- [17] DENG Aidong, BAO Yongqiang, GAO Wei. Research on Fractal Dimension Algorithm of Rub-Impact Acoustic Emission Signal in Rotating Machinery. *Chinese Journal of Scientific Instrument*, 2008, 29(6): 1285-1289.
- [18] Deng Aidong, Tong Hang, Jiang Zhang, Gao Wei. Characteristics of Rub-Impact AE Signals in Rotating Machinery Based on Modal Analysis. *Journal of Southeast University (Natural Science Edition)*, 2010, 40(6):1232-1237.



Acoustic Emission

Edited by Dr. Wojciech Sikorski

ISBN 978-953-51-0056-0

Hard cover, 398 pages

Publisher InTech

Published online 02, March, 2012

Published in print edition March, 2012

Acoustic emission (AE) is one of the most important non-destructive testing (NDT) methods for materials, constructions and machines. Acoustic emission is defined as the transient elastic energy that is spontaneously released when materials undergo deformation, fracture, or both. This interdisciplinary book consists of 17 chapters, which widely discuss the most important applications of AE method as machinery and civil structures condition assessment, fatigue and fracture materials research, detection of material defects and deformations, diagnostics of cutting tools and machine cutting process, monitoring of stress and ageing in materials, research, chemical reactions and phase transitions research, and earthquake prediction.

How to reference

In order to correctly reference this scholarly work, feel free to copy and paste the following:

Deng Aidong and Jiang Zhang (2012). Denoise and Recognition of Friction AE Signal, Acoustic Emission, Dr. Wojciech Sikorski (Ed.), ISBN: 978-953-51-0056-0, InTech, Available from:

<http://www.intechopen.com/books/acoustic-emission/de-noise-and-recognition-of-friction-ae-signal>

INTECH

open science | open minds

InTech Europe

University Campus STeP Ri
Slavka Krautzeka 83/A
51000 Rijeka, Croatia
Phone: +385 (51) 770 447
Fax: +385 (51) 686 166
www.intechopen.com

InTech China

Unit 405, Office Block, Hotel Equatorial Shanghai
No.65, Yan An Road (West), Shanghai, 200040, China
中国上海市延安西路65号上海国际贵都大饭店办公楼405单元
Phone: +86-21-62489820
Fax: +86-21-62489821

© 2012 The Author(s). Licensee IntechOpen. This is an open access article distributed under the terms of the [Creative Commons Attribution 3.0 License](#), which permits unrestricted use, distribution, and reproduction in any medium, provided the original work is properly cited.